Multiband Electromagnetic Wave Absorption Study on Nanocrystalline (1-x)$NiFe_2O_4$/(x)$BaTiO_3$ Composites

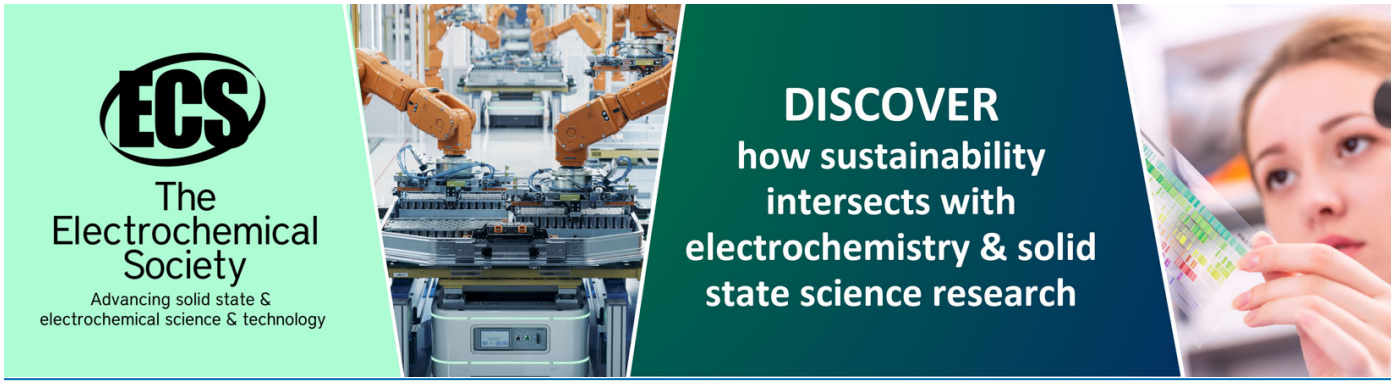

IOP Conf. Series: Journal of Physics: Conf. Series **1436** (2020) 012105 doi:10.1088/1742-6596/1436/1/012105

Multiband Electromagnetic Wave Absorption Study on Nanocrystalline (1-x)$NiFe_2O_4$/(x)$BaTiO_3$ Composites

E. Sukirman[1], Y. Sarwanto[1], S. Ahda[1], Y. Taryana[2] and S. Purwanto[1]

[1] Centre for Science and Technology of Advanced Material-BATAN, Puspiptek, Serpong 15314, Tangerang Selatan, Banten province, Indonesia.
[2] Research Center for Electronics and Telecommunications-LIPI, Jl. Sangkuriang, Bandung 40135, West Java province, Indonesia.

E-mail:engkirs@gmail.com

Abstract. Multiband electromagnetic wave absorption have been studied on nanocrystalline (1-x) $NiFe_2O_4$ (NFO) /(x)$BaTiO_3$ (BTO) composites. The samples were synthesized by solid state reaction using high energy milling (HEM) instrument. The composite samples were characterized using X-ray Diffractometer (XRD) and vibrating sample magnetometer (VSM) instrument. The X-ray diffraction (XRD) patterns of all the samples show single phase and free from impurities. The NFO sample can be indexed to a single cubic crystal structure with a space group of *Fd-3m*, No. 227. While, the BTO sample can be indexed to a single tetragonal crystal structure with a space group of *P4mm*, No. 99. The composite samples consist of two phases, namely NFO and BTO showing soft magnetic performance. The mass magnetization is in the range of 20.0–49.0 emu/g. The electromagnetic parameters of the composites were measured by a vector network analyser in the frequency range of 2 GHz to 18 GHz. The results indicated that (1-x) $NiFe_2O_4$ / (x) $BaTiO_3$ composites display three-band electromagnetic wave absorption. The $0.5NiFe_2O_4$ / $0.5BaTiO_3$ composite displays three-band reflection loss which is larger than the other one and the three-band reflection loss are almost the same, i.e., below the -15 dB. From these experiments it can be concluded that the $0.5NiFe_2O_4$ / $0.5BaTiO_3$ composite is good candidate for electro-magnetic wave absorption.

1. Introduction

Multiferroic composite materials, which possess at least two ferroic properties among ferro-electricity, ferromagnetism, and ferroelasticity are very interesting to be researched and developed. This is because this material has magnetic, optical, electrical and coupling properties between two or more of these properties. This allows the material to be made new and sophisticated RF devices. In addition, the magnetic properties of composites may be easily changed by changing the concentration of magnetic inclusions. Where, for good microwave absorbing performance, one needs a material with high magnitude of permeability, high magnetic loss, a remarkable type of frequency dependence of permeability, and a proper ratio between the permeability and permittivity [1].

Multiferroic exhibit electric, magnetic, and piezoelectric properties. These properties can be coupled to each other resulting in new effects that can be used in a wide range of applications as extremely sensitive ac magnetic field sensors [2], electric-field-controlled magnetic memories [3], tunable microwave devices [4], and a multiband electromagnetic wave absorber device for the RADAR (Radio Detection and Ranging) antidote [5]. Although multiband electromagnetic wave absorption has been an object of study for a long time, there are still rare experimental data using nano precursors. We hope to find new opportunities for developing composites with high microwave permeability and good absorbing performance. Therefore, in this study the multiferroic composite materials were synthesized by the solid state reaction method using the high energy milling (HEM). The purpose of this study was to obtain a multiband electromagnetic wave absorbers based on nanoparticle crystalline of (1-x) $NiFe_2O_4$ / (x) $BaTiO_3$ composites.

2. Experimental Procedure

In this research we have prepared the compounds of $BaTiO_3$ (BTO) and $NiFe_2O_4$ (NFO). BTO was made from the oxide materials of $BaCO_3$ and TiO_2 in powder form, while the NFO was synthesized from NiO and Fe_2O_3 powders. The synthesis procedure in this study is the same as the synthesis method in previous studies **[6]**. In this study, the composite of (1-x) $NiFe_2O_4$ / (x) $BaTiO_3$ were prepared for x = 0.0, 0.34, 0.5, 0.6, and 1.0, hereinafter referred to K1, K2, K3, K4 and K5, respectively. The data of BTO and NFO weight percent in the composite are shown in Table 1.

Table 1. The weight percent of BTO and NFO to be made into composites.

Sample	Weight % of BTO	Weight % of NFO
K1	0	100
K2	34	66
K3	50	50
K4	60	40
K5	100	0

A qualitative analysis with X-ray diffraction technique using X-ray Diffractometer (XRD) was performed. The X-ray diffraction (XRD) patterns were collected on a Powder Diffractometer with using the CuKα-radiation, 40 kV, 40 mA, λ= 1.5406 Å. X-ray diffraction data was analyzed by using GSAS software. The magnetic hysteresis loops were measured with a vibrating sample magnetometer (VSM) (Lakeshore 7300) operating at room temperature. While, the electromagnetic parameters of the composites were measured by a vector network analyser in the frequency range of 2 GHz to 18 GHz

3. Result and discussion

X-ray diffraction data were analyzed by the Rietveld method using GSAS software [**7**]. Peak profiles were fitted using Thompson-Cox-Hastings pseudo-Voigt*Axial divergence asymmetry function with the background mode: 6-coefficients polynomial function. The reliability index of X-ray diffraction patterns analysis depends on the goodness of fit (GOF) parameter, which is stated by χ^2, where the smaller the value, the better is the quality of the fittings. The analysis results from K1, K2, K3, K4, and K5 samples are shown in Figures 1. The X-ray diffraction (XRD) patterns of all the samples show single phase and free from impurities. The dots are the observed intensity, the solid line is the calculated intensity, and the difference pattern is shown at the bottom of the chart.

The sample K1 can be indexed to a single cubic crystal structure of NFO with a space group of *Fd-3m*, No. 227. While, the sample K5 can be indexed to a single tetragonal crystal structure of BTO with a space group of *P4mm*, No. 99. While K2, K3, and K4 is a composite consisting of two phases, namely NFO and BTO. The intensity of NFO peaks increases with increasing its percentage in constituent composite phase and vice versa as the NFO content increases the intensity of BTO decreases. The Rietveld refinement results of atomic coordinate fractions (x_j, y_j, z_j), and occupation factors (g_j), lattice parameters (a, b, c), weight percent (W_t), average crystallite size (D_{av}), indeks reliabilitas (χ^2, R_{wp}), and density (ρ) of K1, K2, K3, K4, and K5 is showed in Table 2 and 3. In these table there are several parameters that cannot be refined, because when refined then the reliability index of chi square, and R_{wp} increases and/or the value of these parameters become abnormal. The initial value of these parameters were taken from Crystallography Open Data (COD) [8] which is then considered as the correct value.

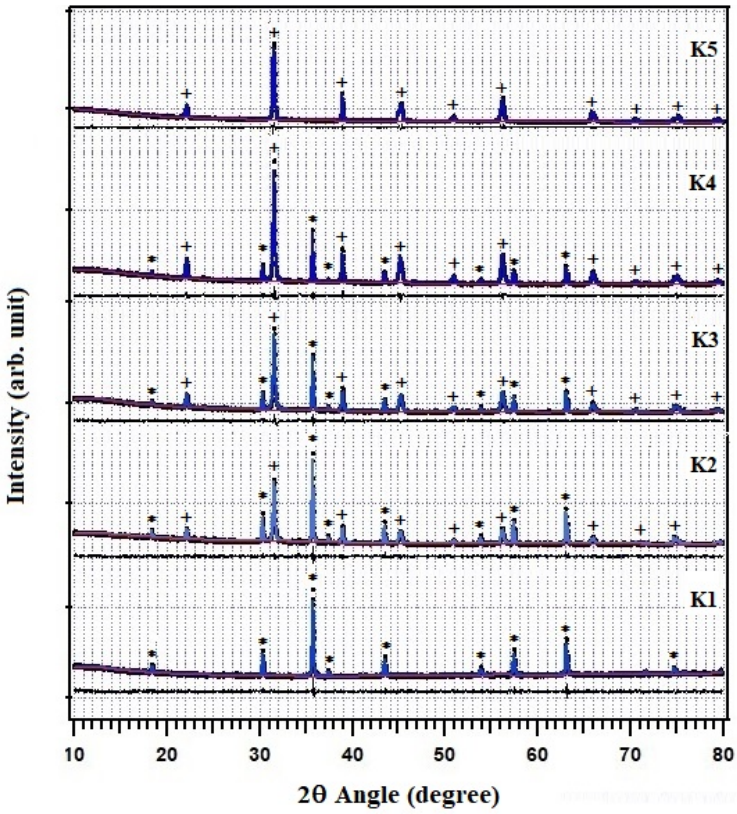

Figure 1. X-ray diffraction pattern analyzed with the Rietveld method using GSAS software in K1, K2, K3, K4, and K5 samples, where * mark the $NiFe_2O_4$ phase and + mark the $BaTiO_3$ phase.

The lattice parameters and of course the NFO unit cell volume is of maximum value when in its own state (K1). But then the NFO lattice parameters are shortened when combined in composite form. Thus, the BTO content in the composite has caused compressive strains induced into the NFO lattice. The crystallite size can be determined by means of XRD indirectly, provided that instrumental broadening is corrected first. For the correction of instrumental broadening, a silicon standard sample with negligible size and strain broadening was run. The peak broadening of the standard sample is exactly the instrumental broadening. The instrumental broadening, then, is used to correct the measured peak broadening, $(\beta_{hkl})_{measured}$ using the relation : $\beta_{hkl} = [(\beta_{hkl})^2_{measured} - (\beta_{hkl})^2_{instrumental}]^{1/2}$.

Therefore, β_{hkl} is the peak broadening due to crystallite size and strain broadening. The mean crystallite size of nanoparticles is obtained through calculations using the Scherrer formulation [**9**]:

$$D = \frac{k\lambda}{\beta \cos\theta} \tag{1}$$

where λ is the X-ray wavelength of CuKα radiation (1.5406 Å), k is the shape factor, to which a value of 0.89 can be assigned if the shape is unknown, θ is the diffraction angle of the peak and β is the width of the half-maximum of the peak. The Williamson–Hall (W–H) plots (as shown in Figure 2 and 3) are drawn for $\boldsymbol{\beta \cos\theta}$ **vs. 4** $\boldsymbol{\sin\theta}$ in order to evaluate micro-strain (ε) and crystallite size (D) using the following relation [**10, 11**]:

$$\beta \cos\theta = \frac{k\lambda}{D} + 4\varepsilon \sin\theta \tag{2}$$

where slope of the straight line is the coefficient 4ε, and ε is micro-strain, while crystallite size is associated with the intercept parameter, $0.9\lambda/D$. This gives the correlation between ε and D values. The average micro-strain (ε) and crystallite size (D_{av}) of $NiFe_2O_4$ in K2, K3, and K4 composite is presented in Table 2. The average micro-strain (ε) and crystallite size (D_{av}) of $BaTiO_3$ in K2, K3, and K4, composite is presented in Table 3.

Table 2. The Rietveld refinement results of atomic coordinate fractions (x_j, y_j, z_j) and occupation factors (g_j), lattice parameters (a, b, c), weight percent (W_t), average crystallite size (D_{av}), indeks reliabilitas (χ^2, R_{wp}), and density (ρ) of **$NiFe_2O_4$** in K1, K2, K3, and K4.

	K1	**K2**	**K3**	**K4**
Parameter	**$NiFe_2O_4$**	**$NiFe_2O_4$**	**$NiFe_2O_4$**	**$NiFe_2O_4$**
Space group	*F d -3 m*	*F d -3 m*	*F d -3 m*	*F d -3 m*
V [Å^3]	578.7(6)	577.21(4)	577.23(5)	577.18(6)
$a = b = c$ [Å]	8.333(2)	8.3261(2)	8.3262(2)	8.3260(3)
Fe1 (8*a*): x_j	0.125	0.125	0.125	0.125
y_j	0.125	0.125	0.125	0.125
z_j	0.125	0.125	0.125	0.125
g_j	0.83(3)	0.9	0.83(5)	0.82(9)
Ni1 (8*a*): x_j	0.125	0.125	0.125	0.125
y_j	0.125	0.125	0.125	0.125
z_j	0.125	0.125	0.125	0.125
g_j	0.100(8)	0.1	0.16(5)	0.06(5)
Fe2 (16*d*): x_j	0.5	0.5	0.5	0.5
y_j	0.5	0.5	0.5	0.5
z_j	0.5	0.5	0.5	0.5
g_j	0.83(3)	0.9	0.74(4)	0.74(8)
Ni2 (16*d*): x_j	0.5	0.5	0.5	0.5
y_j	0.5	0.5	0.5	0.5
z_j	0.5	0.5	0.5	0.5
g_j	0.100	0.1	0.19(4)	0.13(5)
O (32e): x_j	0.255	0.2550(6)	0.256(1)	0.254(1)
y_j	0.255	0.2550(6)	0.256(1)	0.254(1)
z_j	0.255	0.2550(6)	0.256(1)	0.254(1)
g_j	1.0	1.0	1.0	1.0
Wt [%]	100	66.449	51.107	35.914
D_{av} [nm]	**72.9**	138.6	138.6	173.3
ρ (g/cm^3)	5.087	5.348	5.212	4.894
ε [%]	-0.00175	0.025	0.0275	0.0375
χ^2	1.312	1.397	1.568	1.762
R_{wp}	3.07	3.69	4.53	4.88

Table 3. The Rietveld refinement results of atomic coordinate fractions (x_j, y_j, z_j), and occupation factors (g_j), lattice parameters (a, b, c), weight percent (W_t), average crystallite size (D_{av}), indeks reliabilitas (χ^2, R_{wp}), and density (ρ) of **$BaTiO_3$** in K2, K3, K4, and K5.

Parameter	K2 **$BaTiO_3$**	K3 **$BaTiO_3$**	K4 **$BaTiO_3$**	K5 **$BaTiO_3$**
Space group	*P4mm*	*P4mm*	*P4mm*	*P4mm*
V [Å^3]	64.173(8)	64.167(8)	64.01(3)	64.26(3)
$a = b$ [Å]	3.9987(4)	3.9975(2)	3.9942(6)	3.9959(6)
c [Å]	4.0133(8)	4.0153(4)	4.0126	4.0248(6)
Ba (1a): x_j	0.0	0.0	0.0	0.0
y_j	0.0	0.0	0.0	0.0
z_j	0.0	0.0	0.0	0.0
g_j	0.95(5)	0.1(1)	0.92(2)	0.84(1)
Ti (1b): x_j	0.5	0.5	0.5	0.5
y_j	0.5	0.5	0.5	0.5
z_j	0.44(1)	0.47(1)	0.47(1)	0.50(1)
g_j	0.99(7)	0.1(1)	0.92(3)	0.83(1)
O1 (1b): x_j	0.5	0.5	0.5	0.5
y_j	0.5	0.5	0.5	0.5
z_j	0.02(4)	0.0160	0.016	0.016
g_j	1.0	1.0	1.0	1.0
O2 (2c): x_j	0.5	0.5	0.5	0.5
y_j	0.0	0.0	0.0	0.0
z_j	0.52(2)	0.5150	0.52(1)	0.532(9)
g_j	1.0	1.0	1.0	1.0
Wt [%]	33.551	48.893	64.086	100
D_{av} [nm]	154.0	106.6	126.0	**99.0**
ρ (g/cm^3)	5.853	5.404	5.693	5.276
ε [%]	0.135	0.12	0.1375	0.1875
χ^2	1.397	1.568	1.762	1.520
R_{wp}	3.69	4.53	4.88	8.54

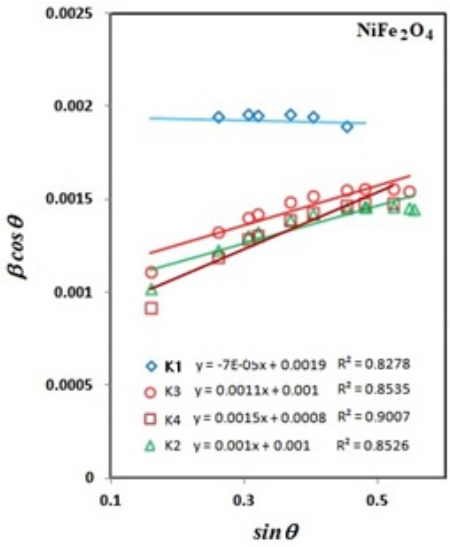

Figure 2. W–H plot of $NiFe_2O_4$ nano-particles.

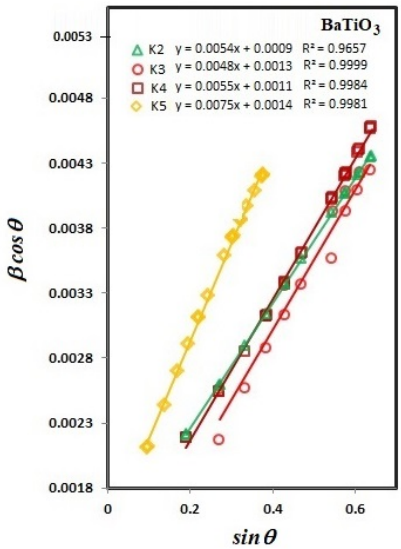

Figure 3. W–H plot of $BaTiO_3$ nano-particles.

The magnetic property measurement of samples K1, K2, K3 and K4 were performed using VSM device. The magnetic hysteresis loops at room temperature versus applied magnetic field up to 1 Tesla are shown in Figure 4. Obviously, all the samples show soft magnetic performance. The mass magnetization is in the range of 20.0 – 49.0 emu/g, while for the pure nickel ferrite (the sample K1), it is 49.0 emu/g. The saturation magnetization (M_s) for the sample K2, K3 and K4 is 36.0, 24.8, and 20.5 emu/g, respectively (Table 4). The results are similar to those obtained in previous studies [**6**, 12]. The M_s of composites goes on decreasing with decreasing in ferrite content. The M_s regularly decrease with increasing BTO content in the sample. This is because M_s is expressed in emu per gram, the less magnetic phase in the sample the smaller the M_s value. Thus, the highest M_s value for the sample K1 is attributed to the absence of $BaTiO_3$ in that sample. The coercivity (H_c) value for the sample K1, K2, K3, and K4 is 111, 177, 177 and 180 Oe, respectively. To clearly compare the H_c values, the zoomed middle part of the hysteresis loops is inserted in the upper right corner of Figure 4.

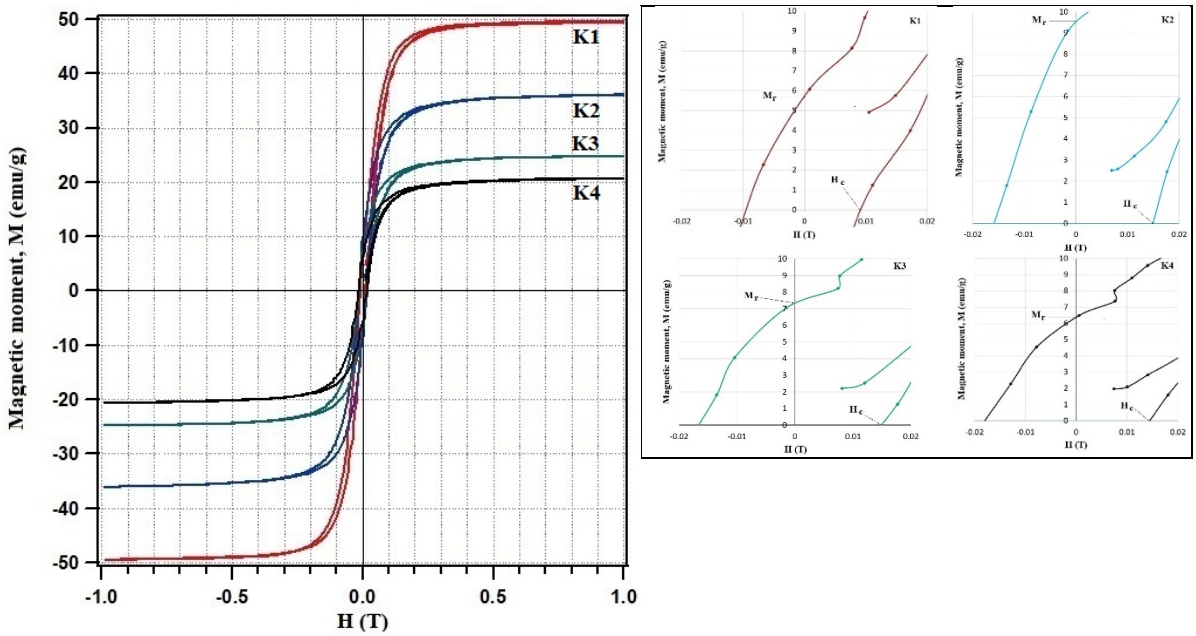

Figure 4. Magnetization curve, M to magnetic field, H from samples of K1, K2, K3, and K4. Zoomed middle part of the hysteresis loops from samples of K1, K2, K3, and K4.

It is shown in Table 2 and 3 that the average crystallite size in the K1 sample is 79.9 nm. Because of its size is smaller than 100 nm, then K1 is fit into the category of nanoparticle materials [**13**]. Therefore, the lowest H_c value of K1 is due to the small size or nanomaterial effect, where the coefficient of nanomaterial is mainly attributed to the demagnetization caused by a single domain rotation [**14**]. Table 4 data shows that the particle sizes of K2 and K3 are the same, which is 138.6 nm. Therefore both samples have the same coercive field, which is 177 Oe.

Table 4. Magnetic parameters of multiferroic composite K-1, K-2, K-3, and K-4.

	Magnetic parameters		
Sample	M_s (emu/g)	M_r (emu/g)	H_c (Oe)
K1	49.0	6.07	111
K2	36.0	9.11	177
K3	24.8	7.06	177
K4	20.5	6.49	180

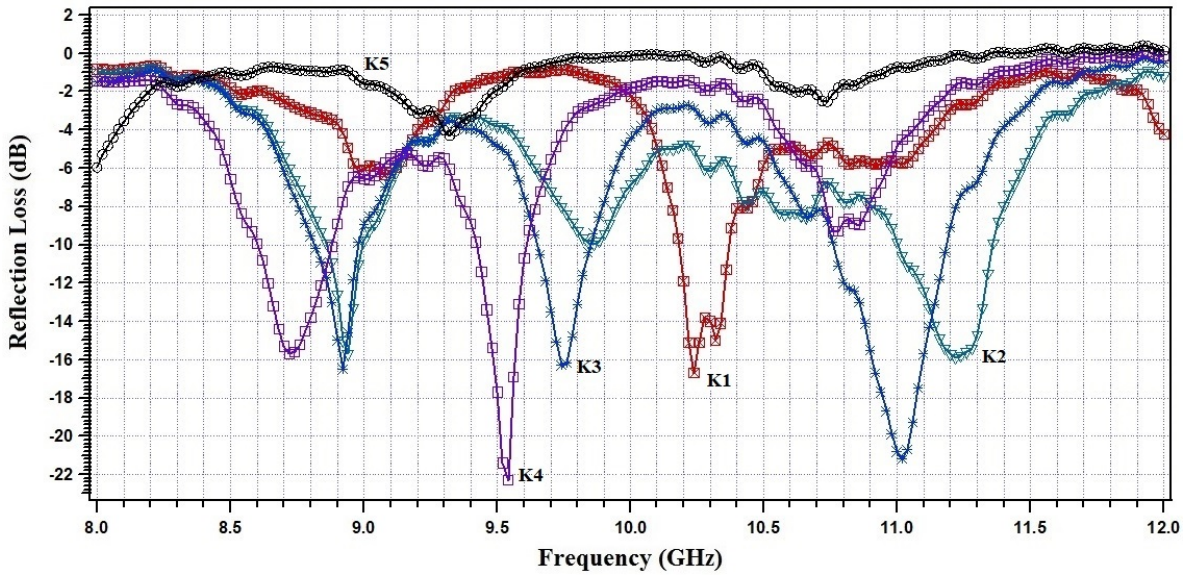

Figure 5. The microwave absorbing characteristics which is stated with parameters reflection loss of the K1, K2, K3, K4 and K5 samples as a frequency function in the range of 8-12 GHz.

H_c characterizes of magnetization reversal of material. The process of reversal is going by 2 main mechanisms: domain walls moving and magnetic rotation of domain magnetic moment. Hc is parameter which strongly dependent on material microstructure and so on particle shapes and sizes. It comes from that facts: (1) a definite size of magnetic domains exist as a result of competition of exchange interaction energy and magnetic interaction energy. When particle sizes decrease, the particles can consists of one domain only and we therefore will not need to provide external energy (by applying external field) for moving of domain walls. (2) crystallographic anisotropy also can decrease with particle size. Thus we will need less external field for rotation of magnetic moment of particle [**15**]. Therefore, the coercivity (H_c) values decrease when we decrease particle size [**16**].

Table 5. The reflection loss of K1, K2, K3, K4 and K5 samples as function of frequency in the range of 8-12 GHz.

	Peak 1		Peak 2		Peak 3	
Sample	f(Hz)	R_L(dB)	f(Hz)	R_L(dB)	f(Hz)	R_L(dB)
K1	9.08	-6.3	10.24	-16.7	11.02	-5.8
K2	8.94	-15.7	9.86	-9.8	11.22	-15.8
K3	8.98	-16.5	9.74	-16.3	11.02	-21.2
K4	8,72	-15.7	9.54	-22.3	10.78	-9.4
K5	8.00	-4.3	9.32	-4.3	10.74	-2.53

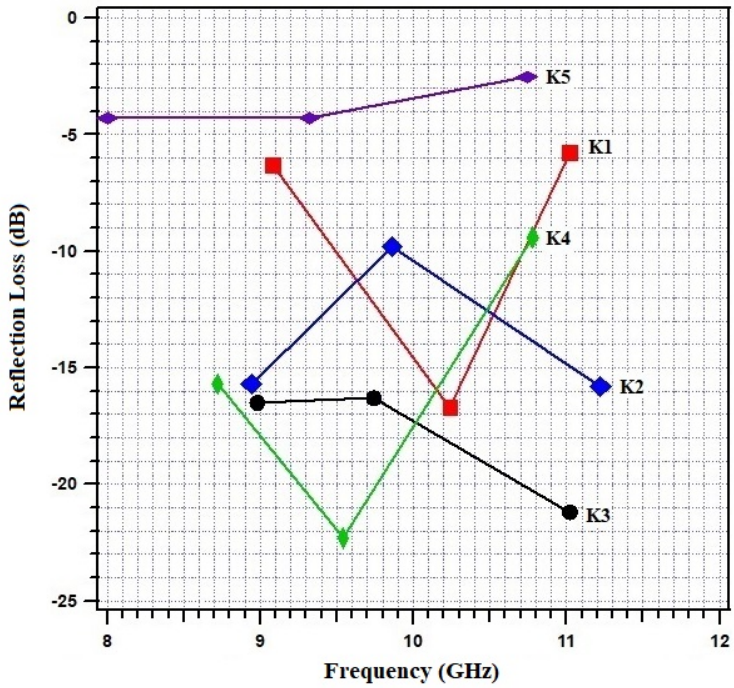

Figure 6. The reflection loss of the K1, K2, K3, K4 and K5 samples as a frequency function in the range of 8-12 GHz.

Reflection loss of (1-x)$NiFe_2O_4$/(x)$BaTiO_3$ composites for x = 0.00, 0.34, 0.50, 0.60 and 1.00 a function of frequency were recorded in the frequency regime of 2–18 GHz shown in Figure 5 and Table 5. It appears that at intervals of 8-12 GHz, the three samples each show three reflection loss valleys. The K3 sample displays reflection loss that is larger and relatively more stable on all three frequency regions, where all three reflection loss points are below the -15 dB figure. Figure 6 illustrates the three reflection loss points of the K1, K2, K3, K4 and K5 samples as a frequency function in the range of 8-12 GHz.

One of the causes of absorption of electromagnetic waves is due to matching impedance. When the material impedance is equal to the characteristic impedance of an electromagnetic wave, maximum absorption will occur. In the K3 sample the impedance value approaching the characteristic impedance of the electromagnetic wave is at the frequencies shown in Table 6.

Table 6. Characteristic impedance, Z (ohm), characteristic frequency, F (GHz) and Reflection Loss, RL (dB) from the K3 sample.

F (GHz)	Z (ohm)	Γ	RL (dB)
8.92	62.6 + j11,4	0.15013	-16.5
9.74	52.6 - j15.7	0.1533	-16.3
11.02	56.6 + j6.57	0.00872	-21.2

From the impedance values in Table 6, it can be seen that in the frequencies of 8.92 GHz and 11.02 GHz, the material is inductive or magnetic in nature, whereas at the frequency of 9.74 GHz, the material is capacitive or electric. From these two conditions, the reflection loss (R_L) value can be calculated by the formula:

$$R_L = 20 \log |\Gamma| \quad (3)$$

where $\Gamma = \left| \frac{Z_{in}-Z_0}{Z_{in}+Z_0} \right|$ is reflection coefficient of material impedance, while Z_{in} and Z_0 are wave impedance of the composite medium and free space, respectively [**17**]. From the above equation, we obtain the value of Γ shown in Table 6. The calculated R_L is equal to the measured one. From the value of R_L, it was concluded that magnetic material has a greater absorption potential compared to electrical ones.

4. Conclusions

(1-x)$NiFe_2O_4$/(x)$BaTiO_3$ composites for x = 0.00, 0.34, 0.50, 0.60 and 1.00 as multiband electromagnetic wave absorber have been successfully synthesized by solid state reaction method using high energy milling. The X-ray diffraction (XRD) patterns of $NiFe_2O_4$ and $BaTiO_3$ samples each show single phase and free from impurities, as well as composite samples consisting of only two phases, namely the $NiFe_2O_4$ and $BaTiO_3$ phases. All of the magnetic samples show soft magnetic performance. The mass magnetization is in the range of 20.0–49.0 emu/g. The microwave absorption properties of these composites in the frequency range of 2 to 12 GHz display three-band electromagnetic wave absorption. The three-band reflection losses of 0.5$NiFe_2O_4$ / 0.5$BaTiO_3$ composite are below -15 dB. From these experiments it can be concluded that the 0.5$NiFe_2O_4$ / 0.5$BaTiO_3$ composite is good candidate for electro-magnetic wave absorption.

Acknowledgements

This research was supported by the DIPA Grants at Centre for Science and Technology of Advanced Materials - National Nuclear Energy Agency, Republic of Indonesia. We would like to thank all those who have helped carry out this R&D activity.

References

[1] Huang L, Liu X and Yu R 2018 *Progress in Natural Science: Materials International* **28**(3) 288.
[2] Sreenivasulu G, Qu P, Petrov V, Qu H and Srinivasan G 2016 *Sensors* (*Basel*) **16**(2) 262.
[3] Wang F, Zhou C, Gesang D and Jiang C 2017 *Nanoscale Res Lett.* **12** 104.
[4] Yang W 2016 *Electric Field Control of Magnetic Properties in Multiferroic Heterostructures* (The University of Sheffield: Dissertation) p 1.
[5]. Sharma V, Rani P, Kunar B. K 2016 *Advanced Materials Proceedings* **1**(1) 65.
[6] Sukirman E, Sarwanto Y, Ahda S and Insani A 2019 Neutron diffraction study on multiferroic 0.6$NiFe_2O_4$/0.4$BaTiO_3$ composite, *Submitted to Makara Journal of Technology*, January 22.
[8] Larson A.C and Von Dreele R.B 1994 *General Structure Analysis System* (GSAS) (Los Alamos National Laboratory Report LAUR 86-748).
[9] Crystallography Open Database 2019 http://www. crystallography.net/cod/, sited April 15.
[10] Ozturk H 2015 *Computational Analysis of Diffraction in Ideal Nanocrystalline Powders* (Columbia University: Dessertation) p. 26.
[11] Thandavan T.M.K, Abdul Gani S.M, Wong C.S, Nor R.M 2017 *J. Nondestruct Eval*. **34** 1.
[12] Singh H.S and Sangwa N 2017 *International J. of Engineering Science Invention* **6**(10) 36.
[13] Khan I, Saeed K, Khan I 2017 *REVIEW Nanoparticles: Properties, applications and toxicities*, Arabian Journal of Chemistry (*Preprint*).
[14] Xu Y, Shen G, Wu H, Liu B 2017 *Materials Science-Poland* **35**(1) 94.
[15] Leitus G 2019 https://www.researchgate.net/post/What_is_the_relationship_between_magnetic_property_and_size_of_the_particle, cited on May 10.
[16] Abdallah H.M.I 2019, https://www.researchgate.net/post/What_is_the_relationship_between_magnetic_property_and_size_of_the_particle, cited on May 10.
[17] Yoshida T, Matsushita M, Morikawa N, Kubota T and Yoshikado S 2017 *Progress In Electrom. Res. Sym.* (Singapore: www.emacademy.org or www.piers.org.).